Available online at www.sciencedirect.com

ScienceDirect

Ceramics International 40 (2014) 3865–3872

CERAMICS INTERNATIONAL

www.elsevier.com/locate/ceramint

Controlling the degradation rate of bioactive magnesium implants by electrophoretic deposition of akermanite coating

Mehdi Razavi[a,c,e,f], Mohammadhossein Fathi[a,b], Omid Savabi[c], Seyed Mohammad Razavi[d], Batoul Hashemi Beni[e], Daryoosh Vashaee[g], Lobat Tayebi[f,h,*]

[a]Biomaterials Research Group, Department of Materials Engineering, Isfahan University of Technology, Isfahan 84156-83111, Iran
[b]Dental Materials Research Center, Isfahan University of Medical Sciences, Isfahan, Iran
[c]Torabinejad Dental Research Center, School of Dentistry, Isfahan University of Medical Sciences, Isfahan 81746-73461, Iran
[d]School of Dentistry, Isfahan University of Medical Sciences, Isfahan 81746-73461, Iran
[e]Department of Anatomical Sciences and Molecular Biology, School of Medicine, Isfahan University of Medical Sciences, Isfahan 81746-73461, Iran
[f]School of Materials Science and Engineering, Helmerich Advanced Technology Research Center, Oklahoma State University, Tulsa, OK 74106, USA
[g]School of Electrical and Computer Engineering, Helmerich Advanced Technology Research Center, Oklahoma State University, Tulsa, OK 74106, USA
[h]School of Chemical Engineering, Oklahoma State University, Stillwater, OK 74078, USA

Received 18 June 2013; received in revised form 6 August 2013; accepted 6 August 2013
Available online 15 August 2013

Abstract

In order to improve the corrosion resistance and the surface bioactivity of biodegradable magnesium alloys, a nanostructured akermanite ($Ca_2MgSi_2O_7$) coating was grown on AZ91 magnesium alloy through electrophoretic deposition (EPD) assisted with micro arc oxidation (MAO) method. The crystalline structures, morphologies and compositions of samples were characterized by X–ray diffraction, scanning electron microscopy and energy dispersive spectroscopy. The in vitro bio–corrosion (biodegradability) and bioactivity behaviors of samples were investigated by electrochemical and immersion tests. The experimental results indicated that the nanostructured akermanite coating could slow down the corrosion rate and improve the in vitro bioactivity of biodegradable magnesium alloy. Thus, magnesium alloy coated with nanostructured akermanite may be a promising candidate to be used as biodegradable bone implants.
Published by Elsevier Ltd and Techna Group S.r.l.

Keywords: D: Glass ceramics; Akermanite coating; Magnesium alloys; Electrophoretic deposition; Degradable implants

1. Introduction

While there are many ongoing investigations in novel implants, the materials that are currently approved to be used include titanium, stainless steel and poly–L–Lactic acid [1–3]. The use of non–degradable metallic implants may require a second surgical operation to remove the implant the implant after the tissue heals [4,5]. Polymer based implants may suffer from poor mechanical strength with limited applications [6].

Magnesium and its alloys have an outstanding strength-to-weight ratio and have been used widely in industrial applications. Magnesium can also be a suitable candidate as an implant material due to its biodegradability, non-toxicity, and excellent mechanical properties, which are similar to the properties of natural bone [7]. Magnesium, as the 11th most abundant element in the body, is essential to almost all living cells, specifically bones [8]. The major drawback of magnesium is its low corrosion resistance in the body, which also influences its mechanical and physical characteristics. Corrosion of magnesium in an aqueous environment can generate a crystalline film of magnesium hydroxide and hydrogen gas. Magnesium also suffers from the chunk effect, which is the detaching of magnesium particles from the bulk material due to hydrogen stress corrosion cracking [9]. Another concern is whether magnesium alloys support the fast precipitation of osteoconductive minerals (bioactivity) after

*Corresponding author at: School of Materials Science and Engineering, Helmerich Advanced Technology Research Center, Oklahoma State University, Tulsa, OK 74106, USA. Tel.: +1 918 594 8634; fax: +1 27 08971179.
E-mail addresses: lobat.tayebi@okstate.edu, lobat.tayebi@gmail.com (L. Tayebi).

0272-8842/$ - see front matter Published by Elsevier Ltd and Techna Group S.r.l.
http://dx.doi.org/10.1016/j.ceramint.2013.08.027

surface modification. Thus, besides improving the corrosion resistance of magnesium alloys, the bioactivity also needs to be improved [10]. Surface modification (e.g. bioceramic coatings) is one of the major techniques to enhance the biocompatibility and bioactivity of implants. Suitable coatings can improve the in vitro bioactivity and protect the implant from fast in vivo corrosion and degradation [11,12].

Silicate biomaterials are known to be applicable for bone tissue repair [13–15]. Among these materials, akermanite ($Ca_2MgSi_2O_7$), a silicate bioceramic with controllable mechanical characteristics and corrosion rate, has attracted recent attention [16,17].

It was shown in previous studies that some cells, such as marrow-derived or adipose-derived stem cells and osteoblasts, have displayed better activities of proliferation and osteogenesis on akermanite than on β-TCP [18–20]. The in vitro and in vivo results suggest the enhanced bioactivity, degradation rate and biocompatibility of the akermanite ceramics. Thus, they can better stimulate the proliferation and differentiation of bone cells. Therefore, they might be used as a potential and attractive bioceramic for bone regeneration, bone tissue engineering, and surface coating applications [21]. In this paper, our aim was to deposit nanostructured akermanite coatings on the surface of magnesium alloy substrates.

To provide a good coating for the implants, it is best if the coating material is in a nonstructural configuration, similar to the crystal morphology of bone minerals [22–25]. Moreover, nanostructured coatings provide more sites for the absorption of ions (e.g., Ca^{2+}, Mg^{2+} and PO_4^{3-}), which resulted in bioactivity and osteoconductivity [26].

There are different methods of developing inorganic coatings on metallic substrates, including plasma spray, sol–gel, enameling, and electrophoretic deposition (EPD) [27–30]. In this paper, we employ the EPD technique for surface modification of our substrate. It is a low cost method that can be performed at room temperature with simple apparatus. The coating time in an EPD procedure is relatively short and the method is adaptable to be used with different materials with various shapes of substrates [31]. In particular, the EPD process could coat uniform layers on the substrates with heterogeneous structures and multipart shapes. Moreover, the thickness of the deposited layers can be adjusted by altering the voltage and the deposition time. Due to all these advantages, EPD techniques are one of the leading methods for surface modification of advanced ceramic materials [32]. To enhance the adhesion strength of the EPD coating, we can coat an intermediate layer between the substrate and the EPD layers using micro arc oxidation (MAO). This intermediate MAO layer is porous and highly adhered to the substrate [33]. The porous structure of the MAO layer provides pinning points for the EPD coating. Moreover, it is known that MAO is a promising method to improve the corrosion resistance of implants as well as their bioactivity [34–36].

The main goal of our study was to increase both the biocorrosion resistance and the in vitro bioactivity of the biodegradable magnesium alloy using a nanostructured akermanite coating on the AZ91 magnesium alloy through EPD assisted with MAO method. More specifically, the MAO was employed to produce a rough and porous structure on the surface of an AZ91 magnesium alloy to provide satisfactory sites for the next layer, which is the EPD of nanostructured akermanite powders.

2. Materials and methods

2.1. Samples preparation

An AZ91 magnesium alloy ingot with 9 wt% aluminum and 1 wt% zinc was used in this work. It was cut into rectangular specimens of $20 \times 15 \times 5\ mm^3$. The samples were ground using SiC papers ranging from 80 to 600 grits. They were ultrasonically rinsed in acetone for 20 min.

2.2. Akermanite preparation

Akermanite powders were prepared by sol–gel process using tetraethyl orthosilicate ($(C_2H_5O)_4Si$, TEOS), magnesium nitrate hexahydrate ($Mg(NO_3)_2 \cdot 6H_2O$) and calcium nitrate tetrahydrate ($Ca(NO_3)_2 \cdot 4H_2O$) as raw materials. Briefly, the TEOS was mixed with water and 2 N HNO_3 (mol ratio: TEOS/H_2O/HNO_3=1:8:0.16) and hydrolyzed for 30 min under stirring. Then, the $Mg(NO_3)_2 \cdot 6H_2O$ and $Ca(NO_3)_2 \cdot 4H_2O$ were added into the mixture (mol ratio:TEOS/$Mg(NO_3)_2 \cdot 6H_2O$/$Ca(NO_3)_2.4H_2O$=2:1:2), and reactants were stirred for 5 h at room temperature. After the reaction, the solution was maintained at 60 °C for 1 day and dried at 120 °C for 2 days to obtain the dry gel [37].

A ball milling process with rotational speed of 250 rpm and ball/powder ratio of 10/1 was carried out for 10 h to prepare the nanostructured akermanite powder.

2.3. MAO process

The electrolyte for the MAO process was composed of 200 g/L NaOH and 200 g/L Na_2SiO_3. We used a power supply in order to perform the procedure. During the MAO process, the AZ91 sample and a stainless steel plate were employed as the anode and the cathode, respectively. The MAO process was carried out at a constant voltage of 60 V for 30 min. Then the samples were ultrasonically rinsed in acetone for 20 min and dried at room temperature.

2.4. Preparation of EPD coating after MAO process

The suspensions were prepared by adding 10 g of nanostructured akermanite powders to 100 mL of organic medium. The medium used in this investigation was methanol. The suspensions were dispersed ultrasonically in an ultrasonic bath for 60 min and then stirred with a magnetic stirrer for 30 min. They were immediately used for EPD procedure without further aging. To deposit the nanostructured akermanite powders on the MAO samples, an electrophoretic cell using the MAO samples as cathode and graphite as anode was connected to an electrophoresis apparatus. The electrodes were

2 cm apart. The deposition voltage was 100 V and the deposition time was 3 min.

2.5. Coatings characterization

In order to identify the phase constituents of AZ91, MAO, akermanite powder and akermanite coated samples, the samples were examined with an X–ray diffractometer (XRD, Philips Xpert) using Ni filtered Cu k_α ($\lambda_{cu\ k\alpha}=0.154186$ nm, radiation at 40 kV) over the 2θ range of 10–90°. We estimated the grain size of prepared akermanite particles by broadening XRD peaks using Williamson–Hall equation [38]:

$$\beta\cos\theta = 0.89\lambda/D + 2\varepsilon\sin\theta \quad (1)$$

where β (rad) is the full width of diffraction, θ (°) is Bragg's angle, λ (nm) is the wavelength of the X–ray peak and 2ε is the slope of the straight line between $\beta\cos\theta$ and $\sin\theta$. The intercept of this line is $0.89\lambda/D$. Thus, we can calculate the grain size, D (nm).

The microstructure and the in vitro bioactivity of AZ91, MAO and akermanite coated samples were studied using a scanning electron microscope (SEM) equipped with energy dispersive spectroscopy (EDS) facilities (Philips XL 30: Eindhoven, The Netherlands).

2.6. Electrochemical measurements

The potentiodynamic polarization experiments and electrochemical impedance spectroscopy (EIS) measurements were performed using an Ametek potentiostat (model PARSTAT 2273) with a three-electrode cell configuration. The saturated calomel electrode was used as a reference and platinum as a counter electrode. The biocompatibility of our samples was evaluated using simulated body fluid (SBF). We used Kokubo's protocol for SBF examinations [39]. All the experiments were performed at the corrosion potential after stabilization (60 min). The potentiodynamic polarization tests were conducted with a scan rate of 1 mV s^{-1}. Also, the scan frequency of EIS measurement ranged from 100 kHz to 10 mHz.

2.7. Immersion test

The immersion test was carried out conforming to the ASTM standard G31. Each sample was immersed in the SBF separately (SBF volume (mL)/sample surface area (cm^2)=10). The temperature of the solution was controlled at 37 °C with a water bath. After 5 different time points of 0, 72, 168, 336, 504 and 672 h, the samples were rinsed with distilled water, acetone, and chromic acid (180 g/L Cr_2O_3) to remove the corrosion products and/or the residual coating on the surface. The samples were then quickly washed with distilled water and dried again, and the final weight was recorded. The weight loss was used to calculate the corrosion rate of the samples by the formula corrosion rate = W/At, in which W, A and t are defined as weight loss, initial surface area exposed to the SBF and the immersion time.

We assessed the in vitro bioactivity of substrates immersed in the SBF (after 72 and 672 h) using the SEM and EDS.

3. Results and discussion

3.1. Coating characterization

XRD patterns of AZ91, MAO, akermanite powder and akermanite coated samples are illustrated in Fig. 1. The only observed peaks in AZ91 spectrum were Mg peaks. The MAO layer was mainly composed of MgO and Mg_2SiO_4. The MgO layer was formed by dissolving Mg^{2+} outward from the substrate and the oxidized oxygen O^{2-} inward from the electrolyte by the reaction (2)

$$Mg^{2+} + O^{2-} \rightarrow MgO \quad (2)$$

Both the SiO_2 and MgO are present in the fused state at high temperature [40]. Though throughout the interval stops of sparking and micro arcing, due to the cooling effect of electrolyte, the fused state SiO_2 and MgO will form the Mg_2SiO_4 according to reaction (3)

$$SiO_2 + 2MgO \rightarrow Mg_2SiO_4 \quad (3)$$

The Mg_2SiO_4 is known as the protective [41,42] and the bioactive [36] filler in MgO as an anodized layer. According to Fig. 1, the initial akermanite powder XRD pattern showed the peaks expected for the akermanite. The strong peaks of akermanite could be seen in the range of 2θ=25–40°. "D" parameter (grain size) is calculated based on Williamson–Hall method as 25 nm which proved the nanostructural pattern of prepared akermanite powder. Based on the XRD pattern of the akermanite coated samples, we can notice the diffraction peaks of MgO, Mg_2SiO_4 and akermanite.

Fig. 2 demonstrates the SEM images of MAO (a,b), akermanite coating (c), and sample's cross–section view (d). Fig. 2a,b indicates the porous and netlike micrograph of MAO. This configuration was made by the molten oxide and gas bubbles emitted out of the micro arc discharge channels. Based on Fig. 2a, b and the XRD data in Fig. 1, both MgO as matrix and the Mg_2SiO_4 as the reinforcing particles can be found in MAO layers. MgO matrix assisted the corrosion resistance, and Mg_2SiO_4 reinforcements facilitated the in vitro bioactivity of the material [36,43]. In addition, due to the porous and netlike structure of the MAO layer, it can provide substantial sites for accommodation of akermanite powders. This will

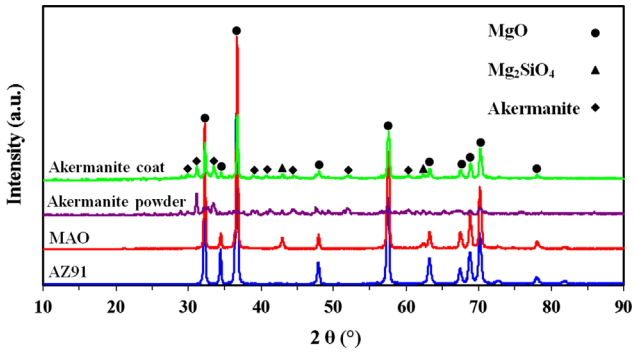

Fig. 1. XRD patterns of AZ91, MAO, akermanite powder and akermanite coated samples.

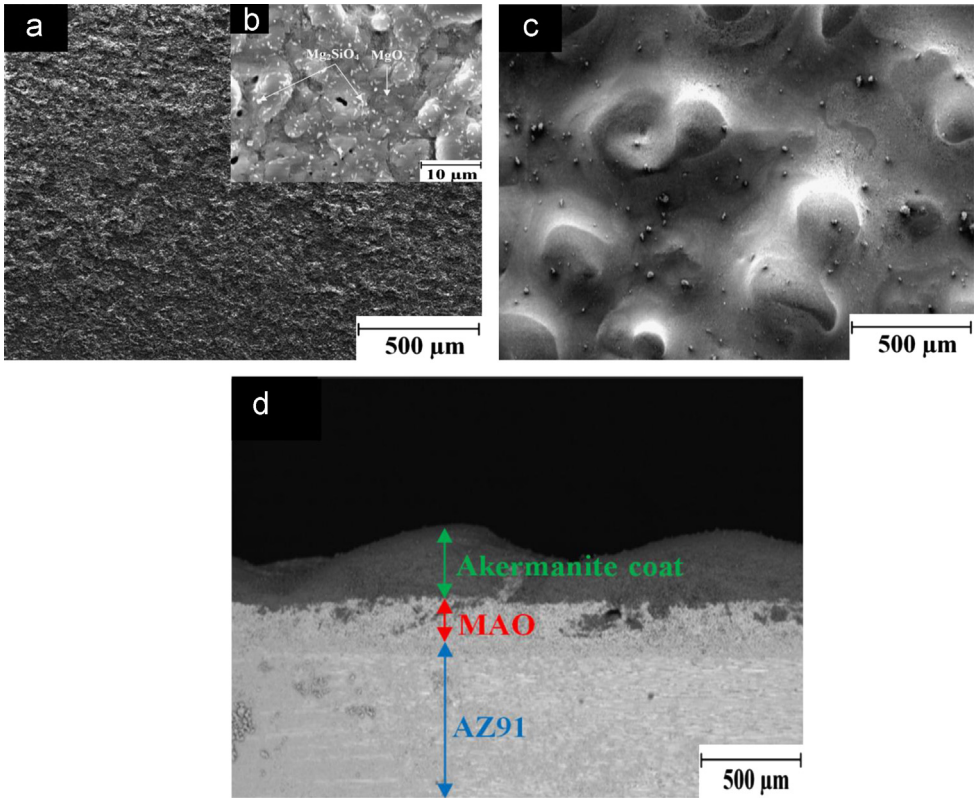

Fig. 2. SEM morphology of MAO (a,b), akermanite coating (c), and sample's cross-section view (d) in different magnifications.

make a suitable substrate for the EPD development. It was previously reported that the adhesion between the MAO and the next coating layer can be enhanced on porous and netlike surfaces [44]. The thickness of the MAO layer and akermanite coating were about 100 and 250 μm, respectively in our construct (Fig. 2d).

Rough and porous surfaces are more suitable for cell attachment and propagation [45]. As can be seen in Fig. 2c, the akermanite coating, which is the outer layer of our implant, was still rough and porous. This makes our substrate appropriate for its function as a bone implant.

3.2. Electrochemical tests

We performed potentiodynamic polarization examinations and electrochemical impedance spectroscopy (EIS) measurements to inspect the protection quality of the AZ91, MAO and akermanite coated samples. Potentiodynamic polarization curves and EIS plots of the AZ91, MAO and akermanite coated samples in the SBF are shown in Fig. 3. Table 1 shows the electrochemical corrosion parameters of the AZ91, MAO and akermanite coated samples. From the potentiodynamic polarization curves, it was found that the corrosion current density (I_{corr}) for the AZ91 substrate increased quickly compared to the MAO and akermanite coated samples. The I_{corr} for the akermanite coated samples was 30 nA/cm^2, which was lower than that of the MAO (53700 nA/cm^2) and AZ91 samples (63,100 nA/cm^2). Compared to the AZ91 sample with −1.6 V E_{corr}, the E_{corr} value for the MAO and akermanite coated samples increased to −1.56 and −1.45 V, respectively. According to the EIS plots, obvious change can be found due to the presence of MAO and akermanite coatings. The capacitance loop diameter of the MAO and akermanite coatings were bigger than that of the AZ91 substrate. Thus, the MAO and akermanite coatings can reduce the corrosion rate of magnesium alloy in the SBF. For simplicity and for the sake of comparison, one might approximately take the real impedance at which the imaginary part vanishes for the capacitive part to be the polarization resistance R_p, and regard it as a measure of corrosion resistance [46]. The EIS data from Nyquist plots reveal that the R_p value increased from 305.5 for the AZ91 sample, to 957.2 for the MAO sample and to 8765.5 Ω for the akermanite coated sample.

In general, the good corrosion resistance can be identified by low corrosion current density, high corrosion potential, and high polarization resistance [47].

In sum, the results of electrochemical tests according to Fig. 3 and Table 1 reveal an improvement of the bio-corrosion property caused by the akermanite coating.

3.3. Immersion test

3.3.1. In vitro bioactivity evaluation

The immersion test was carried out to investigate the in vitro corrosion resistance and bioactivity of AZ91, MAO and akermanite coated samples.

The SEM images of AZ91, MAO and akermanite coated samples after 72 and 672 h immersion in the SBF solution can

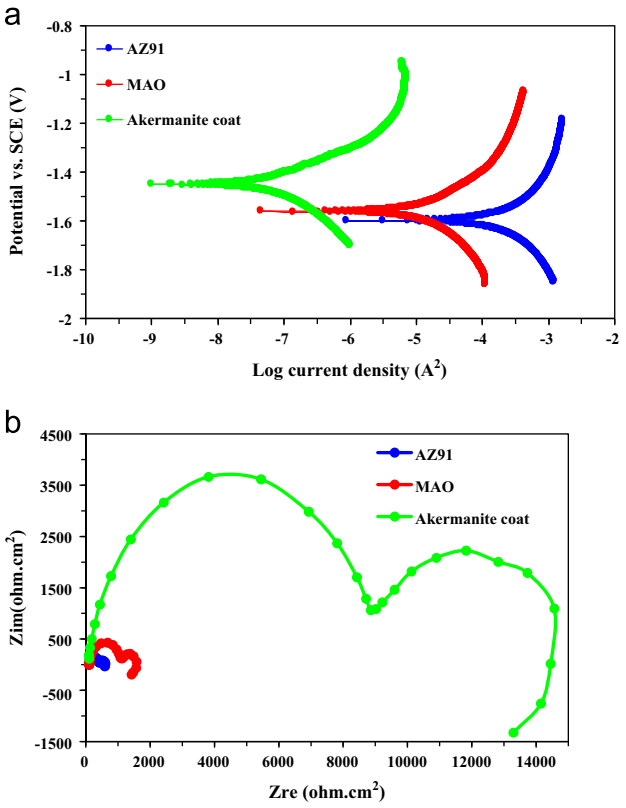

Fig. 3. Polarization (a) and EIS (b) electrochemical tests for the AZ91, MAO and akermanite coated samples in the SBF.

Table 1
Electrochemical corrosion parameters of the AZ91, MAO and akermanite coated samples derived from potentiodynamic polarization experiments and electrochemical impedance spectroscopy (EIS) measurements.

Samples	I_{corr} (nA/cm^2)	E_{corr} (V_{SCE})	R_p (ohm)
AZ91	63,100	−1.6	305.5
MAO	53,700	−1.56	957.2
akermanite coating	30	−1.45	8765.5

be seen in Fig. 4. As shown in this Figure, the surface of AZ91, MAO and akermanite coated samples were cracked and clusters of white particles, which are increasing by the time of immersion, are observable on those surfaces. The AZ91 sample contained more cracks and pits and less white particle precipitations than the other samples. On the other hand, corrosion of the MAO and akermanite coated samples was milder than the AZ91 substrates, which indicates the relatively decent protective layer of these samples. The rate of the corrosion attack and the precipitation of white particles in MAO is between that of the AZ91 and akermanite coated samples (Fig. 4c,d).

By performing an EDS analysis we showed that the cauliflower-like structure in the surfaces of our samples indicated the production of calcium magnesium phosphate [23]. Fig. 5 illustrates the EDS results of white particles in cauliflower-like structure of akermanite coated samples after 672 h immersion in the SBF solution. According to Fig. 5, white particles were mainly composed of Ca, O, Mg, Si and P. The first four elements are presented in the akermanite coating. Though, the presence of P elements in the EDS results, along with the formation of cauliflower-like configuration, can indicate the production of calcium magnesium phosphate. The similarity between these precipitates and the calcium magnesium phosphate of the natural bone indicated the good bioactivity and osteoconductivity of our sample [22–26]

Formation of Mg^{2+} and release of the H_2 bubbles occurs after the immersion of magnesium alloy in the SBF solution. This causes a reaction of NO_3^- and NO_2^- with H^+ and increases the pH value of SBF solution, which facilitates the precipitation of insoluble phosphate [48].

Brushit ($CaHPO_4 \cdot 2H_2O$) can precipitate on the surface of Mg alloy after hydrolye of $Ca(H_2PO_4)_2$. The negative ions such as PO_4^{3-} in the SBF solution can react with the Mg^{2+}, which causes the precipitation of calcium magnesium phosphate. Some proteins, such as fibronectin and vitronectin, that act as cell attachment–promoting proteins can better absorb to the surface at the presence of calcium magnesium phosphate precipitates. This may enhance the cell attachment characteristic of our substrate [49]. Hydrogen bubbles can be formed when the samples corrode. This prevents the adhesion of the precipitates to the substrate [48]. Corrosion of magnesium alloys causes their fast degradation, which is an important drawback to applying those as implants [17]. As we showed, the MAO and akermanite coatings can decrease the corrosion rate of magnesium alloy for biomedical applications.

3.3.2. Corrosion rate evaluation

The corrosion rate of AZ91, MAO and akermanite coated samples can be seen in Fig. 6. All of the samples degraded after immersion in the SBF. The degradation of AZ91 is related to the corrosion reaction of magnesium. However, in other samples the degradation is the result of both the magnesium corrosion and the dissolution of coating layers. We cleaned the sample surface and measured the weight loss as a rate for corrosion. As can be seen in Fig. 6, the corrosion rates of all samples increased during the initial 72 h and then decreased rapidly during the next 96 h followed by a slow decrease during the rest of the procedure. As can be seen in Fig. 6, during the first 72 h, the corrosion rate of akermanite coated samples (0.097 mg/cm^2/hr) is lower than that of the MAO samples (0.38 mg/cm^2/hr) and the corrosion rate of MAO samples is less than that of the AZ91 samples (0.57 mg/cm^2/hr). After 672 h, the corrosion rate of AZ91, MAO and akermanite coated samples decreased to 0.1, 0.06 and 0.019 mg/cm^2/hr, respectively.

In general, due to the electromotive force (EMF) of magnesium, this metal suffers from a high corrosion rate. Chemical dissolution and electrolyte penetration during immersion in the SBF solution facilitates the corrosion procedure.

The reactions that are attributed to the corrosion process of Mg alloys in the SBF solution are as below:

$$Mg_{(s)} + 2H_2O_{(aq)} \rightarrow Mg(OH)_{2(S)} + H_{2(g)} \quad (4)$$

$$Mg(OH)_{2(s)} + 2Cl^-_{(aq)} \rightarrow MgCl_{2(aq)} + 2OH^-_{(aq)} \quad (5)$$

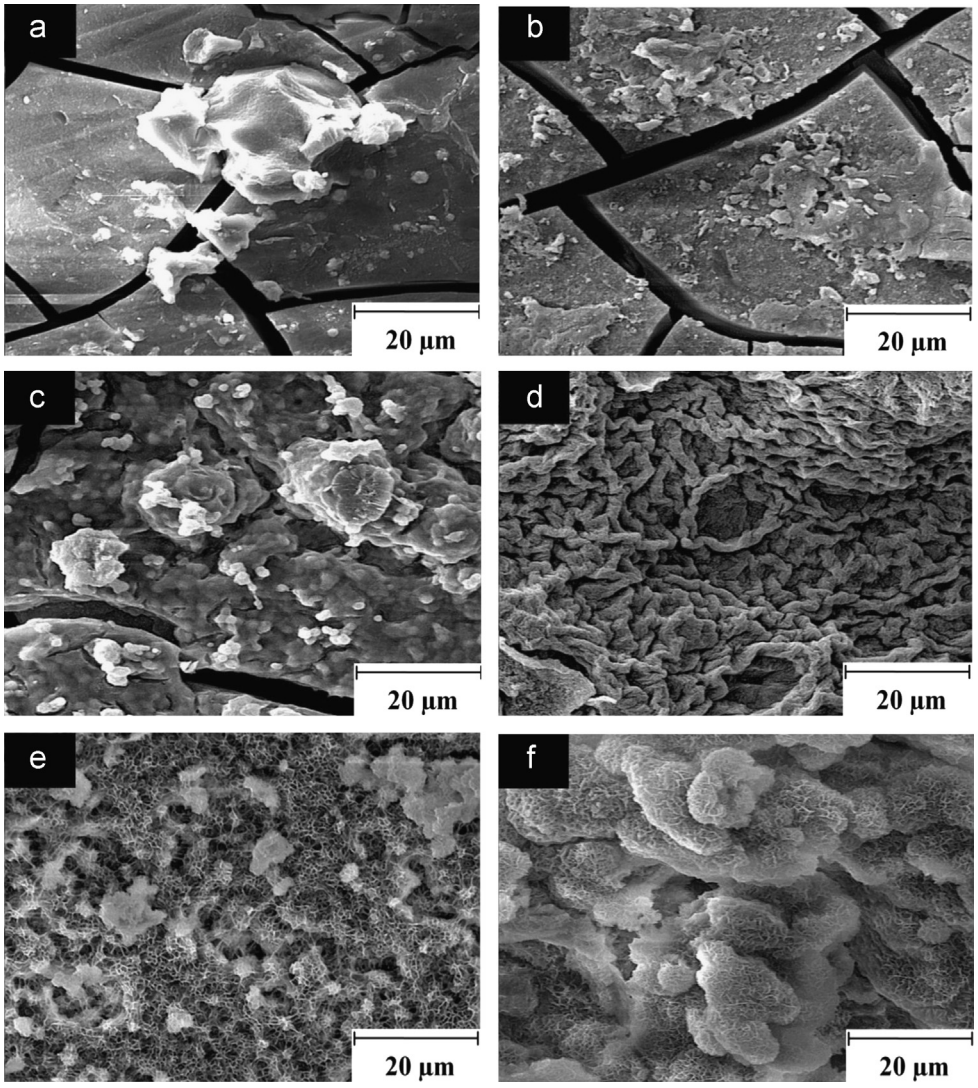

Fig. 4. SEM morphology of the AZ91 (a, b), MAO (c, d) and akermanite coated sample (e, f) samples after 72 h (a, c, e) and 672 h (b, d, f) immersion in the SBF.

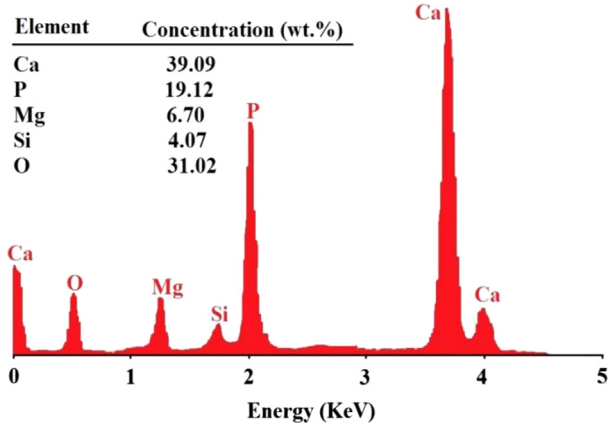

Fig. 5. EDS analysis of precipitated white particles in cauliflower-like structure on the surface of akermanite coated samples after 672 h immersion in the SBF.

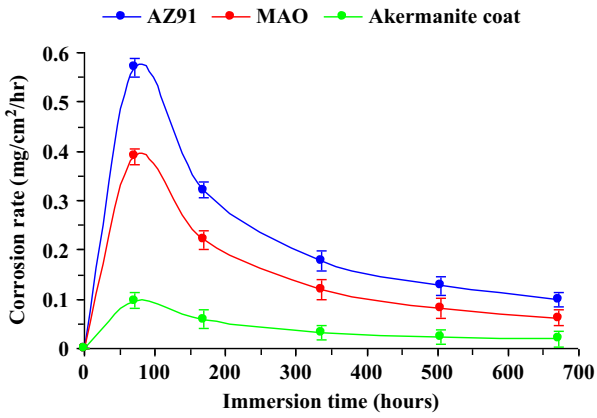

Fig. 6. Corrosion rate of the AZ91, MAO and akermanite coated samples versus immersion time in the SBF.

After production of magnesium hydroxide ($Mg(OH)_2$) in reaction 4, soluble $MgCl_2$ will be formed by reaction of Mg $(OH)_2$ and chloride ions in the SBF solution (reaction (5)) [50].

Since the corrosion products on the surface of the substrate (e.g., $Mg(OH)_2$) can act as the passive layer which were thickening over time, the corrosion rate declines after the primary increase

(Fig. 6) [43]. However, due to the porosity of the $Mg(OH)_2$, the corrosion cannot be completely suppressed and we have slow corrosion to consumption of the total material [51]. Moreover, the precipitation of calcium magnesium phosphate facilitates the decrease of the corrosion rate as well as the increase of in vitro bioactivity of the implants [16–19]. Production of large amounts of calcium magnesium phosphate and other corrosion products is the main reason for the corrosion stabilization at the final stage of our experiments.

4. Conclusion

In this article, the nanostructured akermanite coating was prepared on a biodegradable magnesium alloy by the electrophoretic deposition assisted with the micro arc oxidation method. The bio-corrosion and in vitro bioactivity behaviors of the AZ91, MAO and akermanite coated samples were investigated in the SBF. The following conclusion can be drawn:

The akermanite coating can improve the corrosion resistance and the in vitro bioactivity of magnesium alloys.

Thus, the magnesium alloy coated with the nanostructured akermanite may be a promising candidate to be used as biodegradable bone implants, which deserves further investigation. Controlling the in vivo biodegradation rate and adjusting the mechanical properties of such implants based on the patients' needs are among the topics for future studies.

Acknowledgment

The authors are thankful for the contributions of the Isfahan University of Technology, Torabinejad Dental Research Center, Oklahoma Center for Advancement of Science and Technology (Grant no. AR131-054 8161), AFOSR (Grant no. FA9550-10-1–0010) and the National Science Foundation (NSF, Grant no. 0933763).

References

[1] M.P. Staiger, A.M. Pietak, J. Huadmai, G. Dias, Magnesium and its alloys as orthopedic biomaterials: a review, Biomaterialia 27 (2006) 1728–1734.
[2] G. Song, Control of biodegradation of biocompatible magnesium alloys, Corrosion Science 49 (2007) 1696–1701.
[3] S.K. Tiwari, T. Mishra, M.K. Gunjan, A.S. Bhattacharyya, T.B. Singh, R. Singh, Development and characterization of sol–gel silica–alumina composite coatings on AISI 316L for implant applications, Surface and Coatings Technology 201 (2007) 7582–7588.
[4] A. Pietak, P. Mahoney, G.J. Dias, M.P. Staiger, Bone-like matrix formation on magnesium and magnesium alloys, Journal of Materials Science: Materials in Medicine 19 (2008) 407–415.
[5] O. Rivera–Denizard, N. Diffoot–Carlo, V. Navas, P.A. Sundaram, Biocompatibility studies of human fetal osteoblast cells cultured on gamma titanium aluminide, Journal of Materials Science: Materials in Medicine 19 (2008) 153–158.
[6] N. Kumar, M.N.V. Ravikumar, A.J. Domb, Biodegradable block copolymers, Advanced Drug Delivery Reviews 53 (2001) 23–44.
[7] F. Witte, J. Fischer, J. Nellesen, H.A. Crostack, V. Kaese, A. Pisch, et al., In vitro and in vivo corrosion measurements of magnesium alloys, Biomaterialia 27 (2006) 1013–1018.
[8] F. Witte, N. Hort, C. Vogt, S. Cohen, K.U. Kainer, R. Willumeit, F. Feyerabend, Degradable biomaterials based on magnesium corrosion, Current Opinion in Solid State and Materials Science 12 (2008) 63–72.
[9] Y. Yun, Z. Dong, N. Lee, Y. Liu, D. Xue, X. Guo, et al., Revolutionizing biodegradable metals, Materials Today 12 (2009) 22–32.
[10] Y.W. Song, D.Y. Shan, E.H. Han, Electrodeposition of hydroxyapatite coating on AZ91D magnesium alloy for biomaterial application, Materials Letters 62 (2008) 3276–3279.
[11] J. Li, Y. Song, S. Zhang, C. Zhao, F. Zhang, X. Zhang, et al., In vitro responses of human bone marrow stromal cells to a fluoridated hydroxyapatite coated biodegradable Mg–Zn alloy, Biomaterialia 31 (2010) 5782–5788.
[12] S.R. Paital, N.B. Dahotre, Calcium phosphate coatings for bio-implant applications: materials, performance factors, and methodologies, Materials Science and Engineering R 66 (2009) 1–70.
[13] C. Wu, Y. Ramaswamy, Y. Zhu, R. Zheng, R. Appleyard, A. Howard, et al., The effect of mesoporous bioactive glass on the physiochemical, biological and drug release properties of poly (DL-lactide-co-glycolide) films, Biomaterialia 30 (2009) 2199–2208.
[14] L.L. Hench, Biomaterials: a forecast for the future, Biomaterialia 19 (1998) 1419–1423.
[15] S. Xu, K. Lin, Z. Wang, J. Chang, L. Wang, J. Lu, et al., Reconstructon of calvarial defect of rabbits using porous calcium silicate bioactive ceramics, Biomaterialia 29 (2008) 2588–2596.
[16] C. Wu, J. Chang, Degradation, bioactivity, and cytocompatibility of diopside, akermanite, and bredigite ceramics, Journal of Biomedical Materials Research Part B 83 (2007) 153–160.
[17] T. Kokubo, Bioactive glass ceramics: properties and applications, Biomater 12 (1991) 155–163.
[18] H. Sun, C. Wu, K. Dai, J. Chang, T. Tang, Proliferation and osteoblastic differentiation of human bone marrow–derived stromal cells on akermanite–bioactive ceramics, Biomaterialia 27 (2006) 5651–5657.
[19] Q. Liu, L. Cen, S. Yin, L. Chen, G. Liu, J. Chang, et al., A comparative study of proliferation and osteogenic differentiation of adipose-derived stem cells on akermanite and beta-TCP ceramics, Biomaterialia 29 (2008) 4792–4799.
[20] C. Wu, J. Chang, S. Ni, J. Wang, In vitro bioactivity of akermanite ceramics, Journal of Biomedical Materials Research Part A 76 (2006) 73–80.
[21] Y. Huang, X. Jin, X. Zhang, H. Sun, J. Tu, T. Tang, et al., In vitro and in vivo evaluation of akermanite bioceramics for bone regeneration, Biomaterialia 30 (2009) 5041–5048.
[22] M. Razavi, M.H. Fathi, M. Meratian, Microstructure, mechanical properties and bio–corrosion evaluation of biodegradable AZ91–FA nanocomposites for biomedical applications, Materials Science and Engineering A 527 (2010) 6938–6944.
[23] M. Razavi, M.H. Fathi, M. Meratian, Bio–corrosion behavior of magnesium-fluorapatite nanocomposite for biomedical applications, Materials Letters 64 (2010) 2487–2490.
[24] M. Razavi, M.H. Fathi, M. Meratian, Fabrication and characterization of magnesium–fluorapatite nanocomposite for biomedical applications, Materials Characterization 61 (2010) 1363–1370.
[25] M.H. Fathi, M. Meratian, M. Razavi, Novel magnesium–nano fluorapatite metal matrix nanocomposite with improved biodegradation behavior, Journal of Biomedical Nanotechnology 7 (2011) 1–5.
[26] L. Yang, E.L. Zhang, Biocorrosion behavior of magnesium alloy in different simulated fluids for biomedical application, Materials Science and Engineering C 29 (2009) 1691–1696.
[27] X. Zheng, M. Huang, C. Ding, Bond strength of plasma–sprayed hydroxyapatite/Ti composite coatings, Biomaterialia 21 (2000) 841–849.
[28] I. Singh, C. Kaya, M.S.P. Shaffer, B.C. Thomas, A.R. Boccaccini, Bioactive ceramic coatings containing carbon nanotubes on metallic substrates by electrophoretic deposition, Journal of Materials Science 41 (2006) 8144–8151.
[29] C. Wu, Y. Ramaswamy, D. Gale, W. Yang, K. Xiao, L. Zhang, et al., Novel sphene coatings on Ti–6Al–4V for orthopedic implants using sol–gel method, Acta Biomaterialia 4 (2008) 569–576.
[30] S. Lin, R.Z. LeGeros, J.P. LeGeros, Adherent octacalciumphosphate coating on titanium alloy using modulated electrochemical deposition method, Journal of Biomedical Materials Research 66 (2003) 819–828.

[31] B. Laxmidhar, M. Liu, A review on fundamentals and applications of electrophoretic deposition (EPD), Progress in Materials Science 52 (2007) 1–61.
[32] W. Zhang, X. Chen, X. Liao, Z. Huang, X. Dan, G. Yin, Electrophoretic deposition of porous CaO–MgO–SiO2 glass–ceramic coatings with B_2O_3 as additive on Ti–6Al–4V alloy, Journal of Materials Science: Materials in Medicine 22 (2011) 2261–2271.
[33] W. Shang, B. Chen, X. Shi, Y. Chen, X. Xiao, Electrochemical corrosion behavior of composite MAO/sol–gel coatings on magnesium alloy AZ91D using combined micro–arc oxidation and sol–gel technique, Journal of Alloys and Compounds 474 (2009) 541–545.
[34] D.Q. Wei, Y. Zhou, Y.M. Wang, D.C. Jia, A metasilicate-based ceramic coating formed on magnesium alloy by micro arc oxidation and its corrosion in simulated body fluid, Surface and Coatings Technology 219 (2013) 8–14.
[35] T. Lei, C. Ouyang, W. Tang, L.F. Li, L.S. Zhou, Enhanced corrosion protection of MgO coatings on magnesium alloy deposited by an anodic electrodeposition process, Corrosion Science 52 (2010) 3504–3508.
[36] M. Kharaziha, M.H. Fathi, Synthesis and characterization of bioactive forsterite nanopowder, Ceramics International 35 (2009) 2449–2454.
[37] C. Wu, J Chang, Synthesis and apatite–formation ability of akermanite, Materials Letters 58 (2004) 2415–2417.
[38] G.K. Williamson, W.H. Hall, X-ray line broadening from filed aluminum and wolfram, Acta Metallurgica 1 (1953) 22–31.
[39] T. Kokubo, H. Takadama, How useful is SBF in predicting in vivo bone bioactivity?, Biomateralia 27 (2006) 2907–2915
[40] H.F. Guo, M.Z. An, H.B. Huo, S. Xu, L.J. Wu, Microstructure characteristic of ceramic coatings fabricated on magnesium alloys by micro-arc oxidation in alkaline silicate solutions, Applied Surface Science 252 (2006) 7911–7916.
[41] Y.J. Zhang, C.W. Yan, Development of anodic film on Mg alloy AZ91D, Surface and Coatings Technology 201 (2006) 2381–2386.
[42] H.L. Wu, Y.L. Cheng, L.L. Li, Z.H. Chen, H.M. Wang, Z. Zhang, The anodization of ZK60 magnesium alloy in alkaline solution containing silicate and the corrosion properties of the anodized films, Applied Surface Science 253 (2007) 9387–9394.
[43] X.N. Gu, W. Zheng, Y. Cheng, Y.F. Zheng, A study on alkaline heat treated Mg–Ca alloy for the control of the biocorrosion rate, Acta Biomateralia 5 (2009) 2790–2799.
[44] C. Wu, Z. Wen, C. Dai, Y. Lu, F. Yang, Fabrication of calcium phosphate/chitosan coatings on AZ91D magnesium alloy with a novel method, Surface and Coatings Technology 204 (2010) 3336–3347.
[45] J.L. Xu, F. Liu, F.P. Wang, D.Z. Yu, L.C. Zhao, The corrosion resistance behavior of Al_2O_3 coating prepared on NiTi alloy by micro–arc oxidation, Journal of Alloys and Compounds 472 (2009) 276–280.
[46] I. Epelboin, C. Gabrielli, M. Keddam, H. Takenouti, Electrochemical Corrosion Testing, in: F. Mansferld, U. Betocci (Eds.), ASTM STP 727, ASTM, 1981, p. 150.
[47] X. Cui, Y. Li, Q. Li, G. Jin, M. Ding, F. Wang, Influence of phytic acid concentration on performance of phytic acid conversion coatings on the AZ91D magnesium alloy, Materials Chemistry and Physics 111 (2008) 503–507.
[48] L. Kouisni, M. Azzi, M. Zertoubi, F. Dalard, S. Maximovitch, Phosphate coatings on magnesium alloy AM60 part 1: study of the formation and the growth of zinc phosphate films, Surface and Coatings Technology 185 (2004) 58–67.
[49] B. Feng, J. Weng, B.C. Yang, S.X. Qu, X.D. Zhang, Characterization of titanium surfaces with calcium and phosphate and osteoblast adhesion, Biomateralia 25 (2004) 3421–3428.
[50] Z.J. Li, X.N. Gu, S.Q. Lou, Y.F. Zheng, The development of binary Mg–Ca alloys for use as biodegradable materials within bone, Biomateralia 29 (2008) 1329–1344.
[51] K.Y. Chiu, M.H. Wong, F.T. Cheng, H.C. Man, Characterization and corrosion studies of fluoride conversion coating on degradable Mg implants, Surface and Coatings Technology 202 (2007) 590–598.